J Solid State Electrochem (2009) 13:951–957
DOI 10.1007/s10008-008-0637-9

ORIGINAL PAPER

Crystal structure and electrical conductivity of cubic fluorite-based $(YO_{1.5})_x(WO_3)_{0.15}(BiO_{1.5})_{0.85-x}$ $(0 \leq x \leq 0.4)$ solid solutions

Cheng-Yen Hsieh · Kuan-Zong Fung

Received: 1 July 2007 / Revised: 13 March 2008 / Accepted: 22 July 2008 / Published online: 10 August 2008

Abstract $(WO_3)_{0.15}(BiO_{1.5})_{0.85}$ exhibits a tetragonal structure derived from the fluorite subcell. The electrical conductivity of $(WO_3)_{0.15}(BiO_{1.5})_{0.85}$ is lower than that of Y_2O_3-doped Bi_2O_3. The structure and electrical conductivity of samples formulated as $(YO_{1.5})_x(WO_3)_{0.15}(BiO_{1.5})_{0.85-x}$ (x= 0.1, 0.2, 0.3, and 0.4) were investigated. The as-sintered $(YO_{1.5})_{0.1}(WO_3)_{0.15}(BiO_{1.5})_{0.75}$ exhibited a single cubic structure that is isostructural with δ-Bi_2O_3. For x=0.2, 0.3, and 0.4, the as-sintered samples consisted of a cubic fluorite structure and rhombohedral Y_6WO_{12}. After heat treatment at 600 °C for 200 h, the cubic structures are stable for x=0.1, 0.3, and 0.4. A transformation from cubic to rhombohedral phase after heat treatment at 600 °C for 200 h was observed in the sample originally formulated as $(YO_{1.5})_{0.2}(WO_3)_{0.15}(BiO_{1.5})_{0.65}$.

Keywords Electrolyte · Solid oxide fuel cell · Bismuth oxide

Introduction

In solid oxide fuel cell (SOFC), solid-state electrolytes are defective materials with high ionic conductivity. At present, the common electrolyte material used in solid electrochemical devices is yttria-stabilized zirconia. However, YSZ must be operated above 800 °C to gain high-enough ionic conductivity [1]. Such high-operating temperature would limit its application. Therefore, there is a need to search for a high oxygen ionic conductor that is operative at intermediate temperatures. Up to date, the oxygen ionic conductor with highest ionic conductivity is the high temperature cubic Bi_2O_3, namely, δ-Bi_2O_3, which belongs to the CaF_2 structure [2]. The research for solid state electrolyte based on Bi_2O_3 has been carried out over many years [2–12]. Although δ-Bi_2O_3 possesses quite high oxygen ionic conductivity, the δ phase is not stable below 723 °C. In recent years, several researchers have tried to stabilize the high temperature fluorite structure in Bi_2O_3-based ternary systems. Yaremchenko et al. [13] suggested that the phase transformation at T<900 K is a characteristic of the fluorite-type Bi_2O_3–ZrO_2–Y_2O_3 and Bi_2O_3–Nb_2O_5–Ho_2O_3 solid solutions. Benkaddour et al. [14] suggested that $Bi_{0.85}Pr_{0.105}V_{0.045}O_{1.545}$ exhibits a fcc lattice but shows two domains with different lattice parameter during thermal treatment due to cations and/or anions ordering within the structure in the low temperature range. Lazarraga et al. [15] prepared the cubic $Bi_{1.76}U_{0.12}La_{0.12}O_{3.18}$ at 950 °C, but the cubic phase decomposes to low-symmetry phases after annealing at 600 °C for 100 h. Watanabe [16] investigated $Bi_{3.24}Ln_2W_{0.76}O_{10.14}$ (Ln=La, Pr, and Nd), which exhibits monoclinic cells with pseudo-fcc subcells. Watanabe et al. [17] also reported some compositions of the Bi_2O_3–Er_2O_3–WO_3 system exhibiting δ phase after repetitive long-term heat treatment at 600 °C for 150 h or more. Abrahams et al. [18, 19] investigated Bi_2O_3–WO_3–Nb_2O_5 and Bi_2O_3–Y_2O_3–Nb_2O_5 systems which show a defect fluorite type structure in some compositions. However, it is not clear how these foreign cations affect the structure stability and

C.-Y. Hsieh · K.-Z. Fung (✉)
Department of Materials Science and Engineering,
Frontier Material and Micro/Nano Science
and Technology Center, National Cheng Kung University,
Tainan 70101 Taiwan, Republic of China
e-mail: kzfung@mail.ncku.edu.tw

C.-Y. Hsieh
e-mail: alf@mail.mse.ncku.edu.tw

conduction of Bi_2O_3-based materials. Considering the oxides adopting a fluorite structure, they are commonly formulated as MO_2 where M is the tetravalent cation. As we know, the unit cell of the fluorite-type oxide consists of the so-called M_4O_8 structure. The metal ion is surrounded by eight O ions to form an eightfold coordination structure, and O ion is surrounded by four metal ions to form a tetragonal arrangement. The ratio of metal ionic radius to oxygen ionic radius should be greater than 0.732 in order to form a stable fluorite structure. Although the ratio of Bi ionic radius (1.17 Å [20]) to oxygen ionic radius (1.38 Å [20]) is 0.848, the high oxygen vacancy concentration still destabilizes the fluorite structure. In order to stabilize the fluorite structure, it is needed to reduce average cationic radius or decrease oxygen vacancy concentration. WO_3-doped Bi_2O_3 was found to exhibit stable fluorite-based structures. A solid-solution between 11.9 and 15.15 mol% WO_3-doped Bi_2O_3 exhibits a tetragonal structure. The atomic arrangement of $(WO_3)_{0.125}(BiO_{1.5})_{0.875}$ subcells is similar to that of the fluorite structure [21], but the Bi and W ions do not have random arrangement in these unit cells. The ordered arrangement of cations in $(WO_3)_{0.125}(BiO_{1.5})_{0.875}$ subcells was observed as a result of the large difference in size and valence between Bi and W ions. In this study, the structure of $(YO_{1.5})_x(WO_3)_{0.15}(BiO_{1.5})_{0.85-x}$ (x=0.1, 0.2, 0.3 and 0.4) was carefully examined by X-ray diffraction (XRD). The addition of Y_2O_3 was meant to reduce the mismatch in cation size and valence. The microstructures of these samples were observed using field emission scanning electron microscopy (SEM). The oxygen conductivity was measured using a two-probe technique in air at temperatures ranging from 300 °C to 700 °C.

Experiment procedure

Sample preparation

Solid solutions of Bi_2O_3-based systems were synthesized by a solid-state reaction method using oxides as the raw materials. The adequate amount of Y_2O_3(Showa, 99.99%), and WO_3(Alfa, 99.8%) were mixed with Bi_2O_3(Alfa, 99%), respectively. After ball-milling with ethanol for 24 h, the powder mixtures were dried and sieved through a 200-mesh screen. The mixed powder was calcined in air at 800 °C for 5 h. Subsequently, the powder was pressed into disks. After cold-isostatic pressing at 100 MPa, the disks were sintered in air between 1,000 °C and 1,100 °C for 24 h. The sintered samples were polished by aluminum oxide with particle sizes of 1 and 0.3 μm and followed by thermal etching between 900 °C and 1,100 °C for 3 h.

XRD and SEM analyses

X-ray diffraction data were collected by Rigaku MultiFlex X-ray diffractometer with graphite-monochromated Cu Kα radiation. To examine the structures and lattice parameters, respective samples were analyzed by XRD using a scanning rate of 1°/min at the 2θ range from 20° to 60° and operating at 30 kV, 20 mA. To observe the morphological differences of the synthesized and annealed sample surfaces, the samples were examined using a field emission scanning electron microscopes (FESEM; XL40 FEG PHILIPS) operating at 15 kV with carbon coating. The samples that showed dual phases were analyzed by an energy dispersion X-ray spectrometer (EDAX XL-40135-10).

Conductivity measurement

Platinum electrodes were pasted on the sintered samples and dried at 800 °C for 2 h. Subsequently, the samples were fixed between two Al_2O_3 fixtures, and Ag wires were used to connect Pt electrodes and the multimeter. The conductivity was measured at 300 °C, 400 °C, 500 °C, 600, and 700 °C by a two-probe DC measurement technique, using the HP-34970 multimeter.

Results and discussion

Structure characterization

$(YO_{1.5})_x(WO_3)_{0.15}(BiO_{1.5})_{0.85-x}$ for x= 0

Figure 1 shows the XRD patterns of as-sintered $(YO_{1.5})_x(WO_3)_{0.15}(BiO_{1.5})_{0.85-x}$ for x=(a) 0, (b) 0.1, (c) 0.2, (d) 0.3, and (e) 0.4. Compared with the reflections of (200), (220), (311), (222) from a standard fluorite structure, the splitting of reflections indicates that the as-sintered $(WO_3)_{0.15}(BiO_{1.5})_{0.85}$ exhibited a single tetragonal structure that is isostructural with $(WO_3)_{0.125}(BiO_{1.5})_{0.875}$ [21]. The lattice parameters of $(YO_{1.5})_x(WO_3)_{0.15}(BiO_{1.5})_{0.85-x}$ (x=0, 0.1, 0.2, 0.3 and 0.4) are shown in Table 1. The lattice parameters of $(WO_3)_{0.15}(BiO_{1.5})_{0.85}$ are a=12.52 Å and c=11.26 Å being about $\sqrt{5}$ and 2 times that of δ-Bi_2O_3, (5.66 Å). Apparently, $(WO_3)_{0.15}(BiO_{1.5})_{0.85}$ formed a superstructure consisting of ten enlarged fluorite subcells. The formation of superstructure is caused by an ordered arrangement of W^{6+} and Bi^{3+} cations. The atomic arrangement of superstructured $(WO_3)_{0.15}(BiO_{1.5})_{0.85}$ can be found in the author's previous work [22]. The ordered cation arrangement is simply due to the mismatch in ionic radius and valence.(The ionic radii of Bi and W ions are 1.17 Å [20] and 0.6 Å[20], respectively.) To minimize the

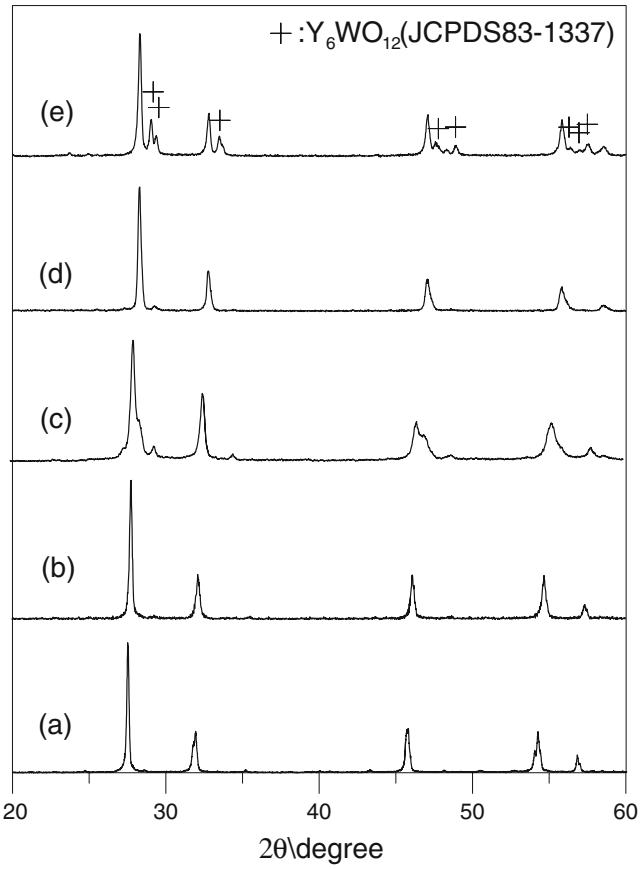

Fig. 1 XRD patterns of as-sintered $(YO_{1.5})_x(WO_3)_{0.15}(BiO_{1.5})_{0.85-x}$ for x=*a* 0, *b* 0.1, *c* 0.2, *d* 0.3, and *e* 0.4

mismatch in ionic radius, it is needed to add foreign cations with ionic radius between Bi and W ions into the cation sublattice of $(WO_3)_{0.15}(BiO_{1.5})_{0.85}$. Trivalent Y ion was found to be the appropriate one.

$(YO_{1.5})_x(WO_3)_{0.15}(BiO_{1.5})_{0.85-x}$ for x= 0.1

The XRD patterns indicated that $(YO_{1.5})_{0.1}(WO_3)_{0.15}(BiO_{1.5})_{0.75}$ exhibits a cubic structure that is isostructural with δ-Bi_2O_3. Therefore, the addition of Y_2O_3 and WO_3 is able to stabilize the high temperature cubic structure of Bi_2O_3 to temperatures below 723 °C. This result suggests that addition of Y_2O_3 causes the random arrangement among Y^{3+}, W^{6+}, and Bi^{3+} cations. Since the ionic radius of Y ion is 1.019 Å [20] and yttria-stabilized bismuth oxide (YSB) forms a cubic solid solution, the addition of Y_2O_3 is capable of minimizing the mismatch in ionic radius between Bi and W ions. Therefore, the co-addition of Y_2O_3 and WO_3 is able to stabilize Bi_2O_3-based cubic structure.

$(YO_{1.5})_x(WO_3)_{0.15}(BiO_{1.5})_{0.85-x}$ for x= 0.2, 0.3, and 0.4

In Fig. 1c, d and e, a second-phase rhombohedral Y_6WO_{12} appeared in the samples $(YO_{1.5})_x(WO_3)_{0.15}(BiO_{1.5})_{0.85-x}$ of x=0.2, 0.3 and 0.4. This result suggests that the solubility limit of Y_2O_3 was between 10 and 20 mol%. In Fig. 1c, XRD traces exhibit shouldering in reflections (111) and (220) for the sample $(YO_{1.5})_x(WO_3)_{0.15}(BiO_{1.5})_{0.85-x}$ of x= 0.2. It is possible that the cubic structure may be stable at high temperature and gradually transform to other structure during the cooling process. This phenomenon was further examined later by long-term heat treatment.

In Fig. 1d and e, the volume fraction of second-phase Y_6WO_{12}, V_2 by XRD was estimated by integrated peak area of Y_6WO_{12} and the cubic phase. The mole fraction, m, was estimated from the volume fraction by XRD as follow:

$$V_2 = \frac{I_2}{I_c + I_2} \tag{1}$$

$$m = \frac{V \times D}{M} \tag{2}$$

Where I_2 and I_c denote the integrated peak area of Y_6WO_{12} and the cubic phase, respectively. D and M denote the theoretical density and molecular weight, respectively. The theoretical density and molecular weight of Y_6WO_{12} are 5.895 g/cm^3 and 909.247. For the samples $(YO_{1.5})_x(WO_3)_{0.15}(BiO_{1.5})_{0.85-x}$ of x=0.3 and 0.4, the theoretical densities are 8.08, 7.5 g/cm^3 and the molecular weights are 393.572, 365.506. From XRD patterns, the volume fractions of second-phase Y_6WO_{12} are 2% and 34% for the samples $(YO_{1.5})_x(WO_3)_{0.15}(BiO_{1.5})_{0.85-x}$ of x=0.3 and 0.4. Therefore, the mole fractions of second phase Y_6WO_{12} are 0.3% and 5.7% in these samples. Finally, the compositions of the cubic phases were estimated to be $(YO_{1.5})_{0.287}(WO_3)_{0.15}(BiO_{1.5})_{0.563}$ and $(YO_{1.5})_{0.125}(WO_3)_{0.154}(BiO_{1.5})_{0.721}$ for the samples $(YO_{1.5})_x(WO_3)_{0.15}(BiO_{1.5})_{0.85-x}$ of x=0.3 and 0.4.

The lattice parameters of the cubic structures

From Table 1, the lattice parameters of the cubic structures decrease with x increasing for the samples $(YO_{1.5})_x(WO_3)_{0.15}(BiO_{1.5})_{0.85-x}$ of x=0.1, 0.2 and 0.3. Since the ionic radius of Y ion is smaller than the ionic radius of Bi ion, the addition of Y_2O_3 tends to reduce the lattice

Table 1 The lattice parameters and activation energies of $(YO_{1.5})_x(WO_3)_{0.15}(BiO_{1.5})_{0.85-x}$ (x=0, 0.1, 0.2, 0.3, and 0.4)

X	Lattice parameters (Å)	Activation energy (kJ/mole)
0	a=12.52, c=11.26	79
0.1	5.56	85
0.2	5.52	86
0.3	5.45	116
0.4	5.45	115

parameter. For the samples $(YO_{1.5})_x(WO_3)_{0.15}(BiO_{1.5})_{0.85-x}$ of x=0.3 and 0.4, the lattice parameters of the cubic structure are nearly identical. From XRD patterns, the compositions of the cubic phases were $(YO_{1.5})_{0.287}(WO_3)_{0.15}(BiO_{1.5})_{0.563}$ and $(YO_{1.5})_{0.125}(WO_3)_{0.154}(BiO_{1.5})_{0.721}$ for the samples $(YO_{1.5})_x(WO_3)_{0.15}(BiO_{1.5})_{0.85-x}$ of x=0.3 and 0.4. The average cation radii of the matrixes are 1.04 and 1.06 Å for the samples $(YO_{1.5})_x(WO_3)_{0.15}(BiO_{1.5})_{0.85-x}$ of x=0.3 and 0.4. Since the average cation radii are nearly the same, the lattice parameters of the cubic phases are reasonably close for the samples $(YO_{1.5})_x(WO_3)_{0.15}(BiO_{1.5})_{0.85-x}$ of x=0.3 and 0.4.

Comparisons between $(YO_{1.5})_x(WO_3)_{0.15}(BiO_{1.5})_{0.85-x}$ and $(LnO_{1.5})_{0.333}(WO_3)_{0.126}(BiO_{1.5})_{0.54}$ (Ln= La, Pr, and Nd)

In recent years, several researchers have tried to stabilize the δ-Bi_2O_3-based structure in ternary systems. Watanabe [16] suggested that $Bi_{3.24}Ln_2W_{0.76}O_{10.14}$ (*Ln*=La, Pr, and Nd) compounds have a monoclinic lattice derived from an fcc lattice, and the formation of the monoclinic phase may be due to the ordering of Bi, *Ln*, and W cations. $Bi_{3.24}Ln_2W_{0.76}O_{10.14}$ can be expressed as a formula of $(LnO_{1.5})_{0.333}(WO_3)_{0.126}(BiO_{1.5})_{0.54}$, which is close to $(YO_{1.5})_{0.3}(WO_3)_{0.15}(BiO_{1.5})_{0.55}$ (x=0.3). However, a second phase Y_6WO_{12} appeared at x=0.2 in this study. Therefore, it may indicate that the solubility limit of Ln_2O_3 (33.3 mol%) in $(LnO_{1.5})_{0.333}(WO_3)_{0.126}(BiO_{1.5})_{0.54}$ is higher than that of Y_2O_3 (between 10 mol% and 20 mol %) in this study. Interestingly, with the addition of approximately same amount of foreign cation into these WO_3–Bi_2O_3 systems, cubic phase was observed in Y_2O_3-added system, but monoclinic phase was found in Ln_2O_3-added system. The ionic radii of La (1.16 Å) [20], Pr (1.126 Å) [20], and Nd (1.109 Å) [20] are larger than that of Y ion (1.019 Å) [13]. On the other hand, the ionic radius of Y^{+3} fall in between that of W^{6+} (0.6 Å) [20] and Bi^{3+} (1.17 Å) [20]. Thus, the addition of Y_2O_3 became more effective on the compensation of mismatch in the cation sublattice.

SEM observation

To verify the results of XRD, the microstructures was further examined by SEM. Figure 2 shows SEM micrographs of thermally etched $(YO_{1.5})_x(WO_3)_{0.15}(BiO_{1.5})_{0.85-x}$ for x=(a) 0.1, (b) 0.2, (c) 0.3, and (d) 0.4. The SEM micrographs clearly show that $(YO_{1.5})_x(WO_3)_{0.15}(BiO_{1.5})_{0.85-x}$ (x=0.1, 0.2, 0.3, and 0.4) are composed of two phases. Two types of grains are clearly observed as shown in Figure 2. The needle-like grains appeared at grain boundaries of the larger grains. The amount of needle-like phase increase with increasing Y ion content. It is difficult to quantitatively analyze the small needle-like grains without interference from the larger grains. However, the needle-like grains have more Y content than the large grain based on EDX results. Therefore, it is suggested that the composition of needle-like grains corresponds to the second phase Y_6WO_{12}. For the sample $(YO_{1.5})_x(WO_3)_{0.15}(BiO_{1.5})_{0.85-x}$ of x=0.1, the volume fraction of second phase Y_6WO_{12} is only 2.5% from SEM micrograph. However, the absence of Y_6WO_{12} reflection in XRD trace (Fig. 1) may result from the low instrument sensitivity of XRD.

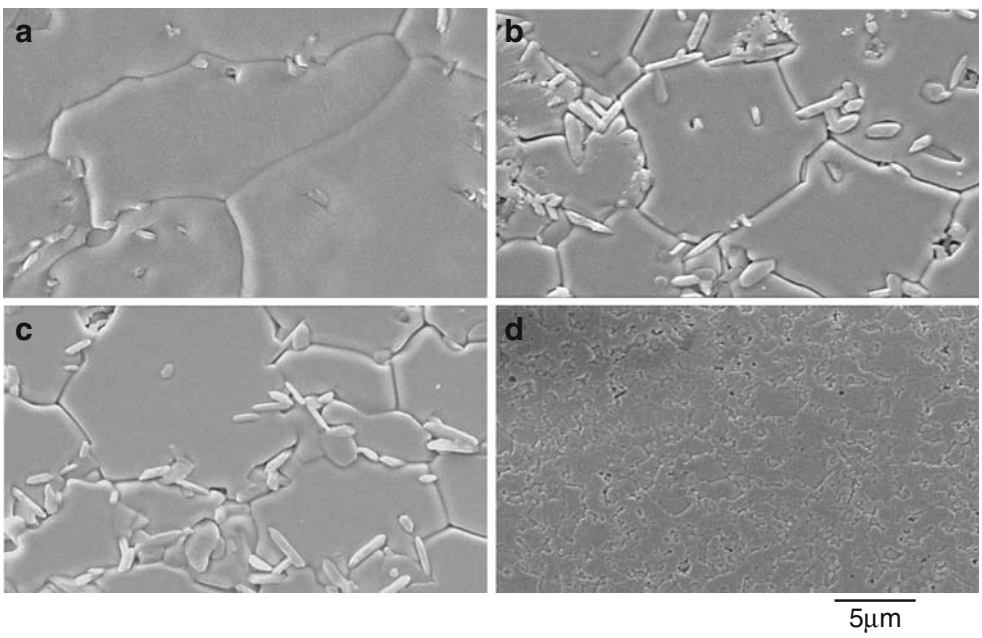

Fig. 2 SEM micrographs of thermal-etched $(YO_{1.5})_x(WO_3)_{0.15}(BiO_{1.5})_{0.85-x}$ for x=**a** 0.1, **b** 0.2, **c** 0.3, and **d** 0.4

Thermal stability after heat treatment at 600 °C

The cubic yttria-stabilized bismuth oxide is known as a metastable phase and may transform from cubic to hexagonal phase after heat treatment at 600 °C[7]. Thus, the stabilization of isotropic high temperature cubic phase in this study was further examined by long-time heat treatment. Figure 3 shows XRD patterns of $(YO_{1.5})_x(WO_3)_{0.15}(BiO_{1.5})_{0.85-x}$ for x=(a) 0.1, (b) 0.2, (c) 0.3, and (d) 0.4 after heat treatment at 600 °C for 200 h. The structures are stable after heat treatment at 600 °C for 200 h for the samples $(YO_{1.5})_x(WO_3)_{0.15}(BiO_{1.5})_{0.85-x}$ of x=0.1, 0.3 and 0.4. However, for the sample $(YO_{1.5})_x(WO_3)_{0.15}(BiO_{1.5})_{0.85-x}$ of x=0.2 after heat treatment at 600 °C for 200 h in Figure 3 (b), the splitting and shouldering of reflections of (111), (220), and (311), based on a standard fluorite structure, indicate that a phase transformation occurred. Therefore, the single cubic structure in $(YO_{1.5})_x(WO_3)_{0.15}(BiO_{1.5})_{0.85-x}$ of x=0.2 is metastable. To further examine the phase transformation for the sample $(YO_{1.5})_x(WO_3)_{0.15}(BiO_{1.5})_{0.85-x}$ of x=0.2, the sample was heated at 600 °C for 1,000 h. The XRD pattern of Fig. 4 indicated that the sample $(YO_{1.5})_x(WO_3)_{0.15}(BiO_{1.5})_{0.85-x}$ of x=0.2 exhibits two cubic structures and Y_6WO_{12} after heat treatment at 600 °C for 1,000 h. The lattice parameters of two cubic structures are 5.52 and 5.45 Å which is the same as that of the cubic structure for the sample $(YO_{1.5})_x(WO_3)_{0.15}(BiO_{1.5})_{0.85-x}$ of x=0.3. It is suggested that the composition of the second cubic structure is the same as that for the sample $(YO_{1.5})_x(WO_3)_{0.15}(BiO_{1.5})_{0.85-x}$ of x=0.3, so the composition may be $(YO_{1.5})_{0.287}(WO_3)_{0.15}(BiO_{1.5})_{0.563}$.

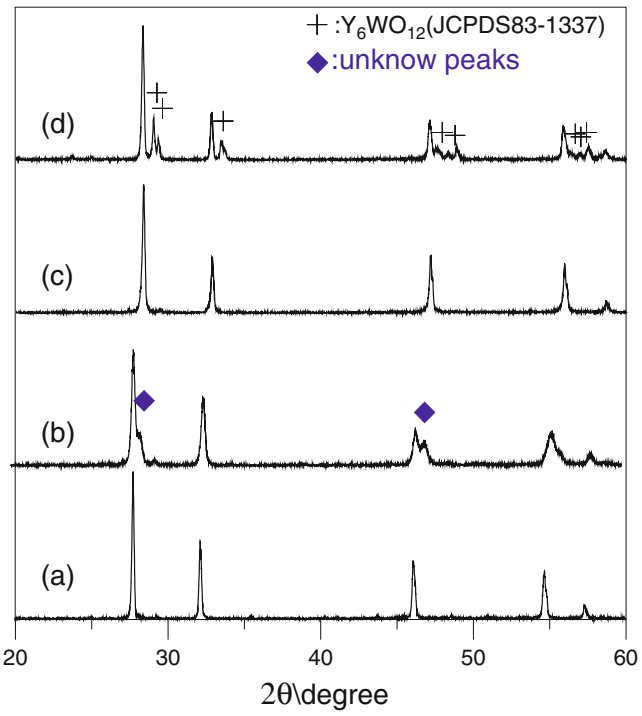

Fig. 3 XRD patterns of $(YO_{1.5})_x(WO_3)_{0.15}(BiO_{1.5})_{0.85-x}$ for x=*a* 0.1, *b* 0.2, *c* 0.3, and *d* 0.4 after annealing at 600 °C for 200 h

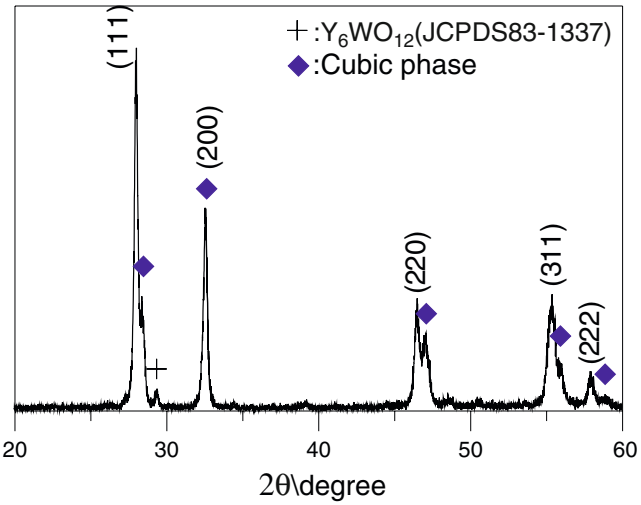

Fig. 4 XRD patterns of $(YO_{1.5})_x(WO_3)_{0.15}(BiO_{1.5})_{0.85-x}$ for x=0.2 after annealing at 600 °C for 1000 h

As mentioned above, reducing average cationic radius or decreasing oxygen vacancy concentration are two common approaches to stabilize the cubic fluorite bismuth oxide. In order to stabilize the cubic structure, several researchers [13–15] tried to add cations which values are higher than 3 into the lanthanoid oxide doped Bi_2O_3. Although the as sintered $(Bi_{1-x}Nb_x)_{1-y}Ho_yO_{1.5+\delta}$ (x=0.05 and 0.08; y= 0.10–0.15) [15], $(Bi_{1-x}Zr_x)_{1-y}Y_yO_{1.5+\delta}$ (x=0.05 and 0.07; y=0.15) [13], $Bi_{0.85}Pr_{0.105}V_{0.045}O_{1.545}$ [14], and $Bi_{1.76}U_{0.12}La_{0.12}O_{3.18}$ [15] exhibit a cubic structure. Theoretically, the oxygen vacancy concentrations of these systems are still over 20%. Such high oxygen vacancy concentration is detrimental to the stability of the fluorite structure. Therefore, the phase transformation still occurred in these systems after long-term heat treatment below 600 °C. Watanabe et al. [17] reported that $(Bi_2O_3)_x(Er_2O_3)_y(WO_3)_z$ ($x+y+z$=1) with low W content such as $(Bi_2O_3)_{0.745}(Er_2O_3)_{0.205}(WO_3)_{0.05}$ showed δ phase. The oxygen vacancy concentrations of $(Bi_2O_3)_{0.745}(Er_2O_3)_{0.205}(WO_3)_{0.05}$ is 23.15%, and δ phase is stable after repetitive long-term heat treatment at 600 °C for 150 h or more. It is suggested that the addition of the smaller ions Er and W ions into Bi_2O_3 is capable of stabilizing the fluorite structure and maintaining the high oxygen vacancy concentration.

In this study, the addition of 15 mol% WO_3 can reduce the average cationic radius obviously. Theoretically, the oxygen vacancy concentration of $(YO_{1.5})_x(WO_3)_{0.15}(BiO_{1.5})_{0.85-x}$ is a constant being 13.75%. The decrease of the oxygen vacancy concentration and the average cationic

radius is favorable to stabilize the fluorite structure. From XRD patterns of Fig. 3, the cubic structures of $(YO_{1.5})_x(WO_3)_{0.15}(BiO_{1.5})_{0.85-x}$ are stable after heat treatment at 600 °C for 200 h for the samples $(YO_{1.5})_x(WO_3)_{0.15}(BiO_{1.5})_{0.85-x}$ of x=0.1, 0.3, and 0.4. Therefore, reducing average cationic radius and decreasing oxygen vacancy concentration are really helpful to stabilize the cubic fluorite bismuth oxide. As mentioned above, two cubic phases after heat treatment at 600 °C for 1,000 h was observed for the sample $(YO_{1.5})_x(WO_3)_{0.15}(BiO_{1.5})_{0.85-x}$ of x=0.2 in Fig. 4. The composition of the second cubic structure may be $(YO_{1.5})_{0.287}(WO_3)_{0.15}(BiO_{1.5})_{0.563}$. Therefore, the composition of the cubic structure for the sample $(YO_{1.5})_x(WO_3)_{0.15}(BiO_{1.5})_{0.85-x}$ of x=0.2 lies in binary phase zone between cubic $(YO_{1.5})_{0.1}(WO_3)_{0.15}(BiO_{1.5})_{0.75}$ and cubic $(YO_{1.5})_{0.287}(WO_3)_{0.15}(BiO_{1.5})_{0.563}$.

Conductivity characterization

Figure 5 shows the conductivities of $(YO_{1.5})_x(WO_3)_{0.15}(BiO_{1.5})_{0.85-x}$ for x=(a) 0, (b) 0.1, (c) 0.2, (d) 0.3, and (e) 0.4. For the samples $(YO_{1.5})_x(WO_3)_{0.15}(BiO_{1.5})_{0.85-x}$ of x=0.1 and 0.2, the conductivities are higher than that of $(WO_3)_{0.15}(BiO_{1.5})_{0.85}$. For the samples $(YO_{1.5})_x(WO_3)_{0.15}(BiO_{1.5})_{0.85-x}$ of x=0.2, 0.3, and 0.4, the conductivities decreased as x increased. An oxide with CaF_2 structure may be expressed as AO_2. Addition of an Y_2O_3 in AO_2 increased an oxygen vacancy. But there was 25 mol% oxygen vacancy concentration in δ-Bi_2O_3. Therefore, the substitution of Y^{+3} for Bi^{+3} did not change the oxygen vacancy concentration. Theoretically, the conductivities of

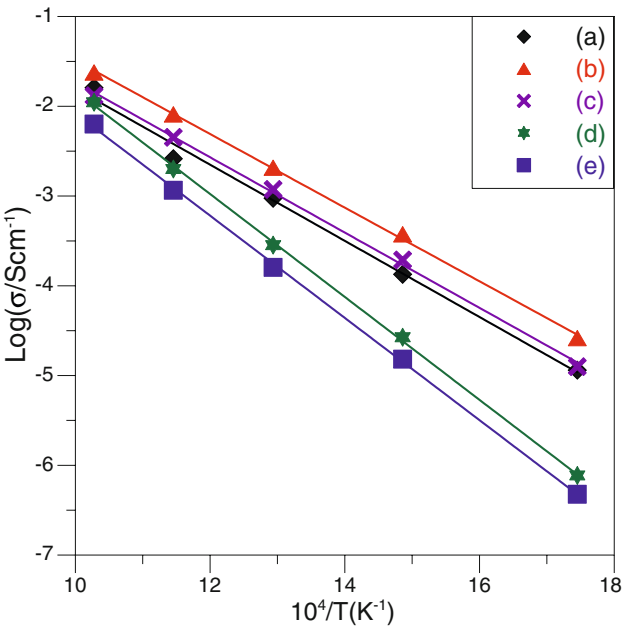

Fig. 5 Conductivities of $(YO_{1.5})_x(WO_3)_{0.15}(BiO_{1.5})_{0.85-x}$ for x=*a* 0, *b* 0.1, *c* 0.2, *d* 0.3, and *e* 0.4

$(YO_{1.5})_x(WO_3)_{0.15}(BiO_{1.5})_{0.85-x}$ should not change significantly. For the samples $(YO_{1.5})_x(WO_3)_{0.15}(BiO_{1.5})_{0.85-x}$ of x=0.2, 0.3, and 0.4, a second phase Y_6WO_{12} appeared, and the conductivity decreased as x increased. For the sample $(YO_{1.5})_x(WO_3)_{0.15}(BiO_{1.5})_{0.85-x}$ of x=0.1, the cubic structure is more symmetric than the tetragonal structure of $(WO_3)_{0.15}(BiO_{1.5})_{0.85}$. Thus, the conductivity is $2.38\times10^{-}$ S cm^{-1} at 700 °C which is higher than that of $(WO_3)_{0.15}(BiO_{1.5})_{0.85}$($1.5\times10^{-2}$ S cm^{-1}).

The conductivity of $(YO_{1.5})_{0.1}(WO_3)_{0.15}(BiO_{1.5})_{0.75}$ is also higher than that of the monoclinic $(LnO_{1.5})_{0.333}(WO_3)_{0.126}(BiO_{1.5})_{0.54}$ (*Ln* = La, Pr, and Nd) [16] compounds due to the symmetric cubic structure. The oxygen vacancy concentration of $(YO_{1.5})_{0.1}(WO_3)_{0.15}(BiO_{1.5})_{0.75}$ (13.75%) is less than that of the $(Bi_{1-x}Nb_x)_{1-y}Ho_yO_{1.5+\delta}$ (x=0.05 and 0.08; y=0.10–0.15) [13], $(Bi_{1-x}Zr_x)_{1-y}Y_yO_{1.5+\delta}$ (x=0.05 and 0.07; y=0.15) [13], $Bi_{0.85}Pr_{0.105}V_{0.045}O_{1.545}$ [14], $Bi_{1.76}U_{0.12}La_{0.12}O_{3.18}$ [15], and $(Bi_2O_3)_{0.745}(Er_2O_3)_{0.205}(WO_3)_{0.05}$ (over 20 mol%) [17]. Therefore, the conductivity of $(YO_{1.5})_{0.1}(WO_3)_{0.15}(BiO_{1.5})_{0.75}$ is lower than that of those systems. The activation energies of $(YO_{1.5})_x(WO_3)_{0.15}(BiO_{1.5})_{0.85-x}$ (x=0, 0.1, 0.2, 0.3 and 0.4) are shown in Table 1. For the samples $(YO_{1.5})_x(WO_3)_{0.15}(BiO_{1.5})_{0.85-x}$ of x=0, 0.1 and 0.2, the activation energies are about the same. When x is greater than 0.3, the activation energies increase obviously. Moreover, Laarif et al. [6] suggested that the Bi $6s^2$ lone pairs of electrons resulted in high polarizability of the cation network, which leads to oxygen ion mobility. Yttrium ion, on the other hand, did not show any lone pair electrons. Thus, it is reasonable to expect that ionic conductivity drops and the activation energies increase as Y is substituted for Bi. Moreover, the lattice parameters of the cubic fluorite structure decreased with increasing Y content that also suppressed the oxygen ion mobility.

Conclusions

The as-sintered $(YO_{1.5})_{0.1}(WO_3)_{0.15}(BiO_{1.5})_{0.75}$ consists of a cubic fluorite structure and a very small amount of rhombohedral Y_6WO_{12} based on SEM observation. For the samples $(YO_{1.5})_x(WO_3)_{0.15}(BiO_{1.5})_{0.85-x}$ of x=0.2, 0.3 and 0.4, the as-sintered samples also are not single-phased and consist of a cubic fluorite structure and rhombohedral Y_6WO_{12}. After heat treatment at 600 °C for 200 h, two cubic phases was observed for $(YO_{1.5})_x(WO_3)_{0.15}(BiO_{1.5})_{0.85-x}$ of x=0.2. The composition of the cubic structure for the sample $(YO_{1.5})_x(WO_3)_{0.15}(BiO_{1.5})_{0.85-x}$ of x=0.2 lies in binary phase zone between cubic $(YO_{1.5})_{0.1}(WO_3)_{0.15}(BiO_{1.5})_{0.75}$ and cubic $(YO_{1.5})_{0.287}(WO_3)_{0.15}(BiO_{1.5})_{0.563}$. For the sample $(YO_{1.5})_x(WO_3)_{0.15}(BiO_{1.5})_{0.85-x}$ of x=0.1, the cubic structure is more symmetric than the

tetragonal structure of $(WO_3)_{0.15}(BiO_{1.5})_{0.85}$. Thus, the conductivity is 2.38×10^{-2} S cm^{-1} at 700 °C and slightly higher than that of $(WO_3)_{0.15}(BiO_{1.5})_{0.85}$. For the samples $(YO_{1.5})_x(WO_3)_{0.15}(BiO_{1.5})_{0.85-x}$ of x=0.2, 0.3 and 0.4, a second-phase Y_6WO_{12} appeared, and the conductivity decreased with increasing x value. Although the oxygen vacancy concentration was the same with increasing x, the decrease in Bi $6s^2$ lone pairs of electrons blocks oxygen ion mobility. Thus, it is reasonable to expect that ionic conductivity drops as Y is substituted for Bi.

Acknowledgments This work is supported by the Council of Agriculture, Executive Yuan R. O. C. under the grant No. 96AS-10.1.1-AD-U1.

References

1. Etsell TH, Flengas SN (1970) Chem Rev 70:339
2. Harwig HA, Gerards AG (1978) J Solid State Chem 26:265
3. Rao CNR, Subba Rao GV, Ramdas S (1969) J Phys Chem 73:672
4. Azad AM, Larose S, Akbar SA (1994) J Mater Sci 29:4135
5. Shuk P, Wiemhöfer HD, Guth U, Göpel W, Greenblatt M (1996) Solid State Ionics 89:179
6. Laarif A, Theobald F (1986) Solid State Ionics 21:183
7. Kruidhof H, DeVries KJ, Burggraaf AJ (1990) Solid State Ionics 37:213
8. Takahashi T, Iwahara H (1978) Mater Res Bull 13:1447
9. Takahashi T, Iwahara H, Esaka T (1977) J Electrochem Soc 124:1563
10. Hoda SN, Chang LLY (1974) J Am Ceram Soc 57:323
11. Wachsman ED, Ball GR, Jiang N, Stevenson DA (1992) Solid State Ionics 52:213
12. Sammes NM, Gainsford GJ (1993) Solid State Ionics 62:179
13. Yaremchenko AA, Kharton VV, Naumovich EN, Tonoyan AA, Samokhval VV (1998) J Solid State Electrochem 2:308
14. Benkaddour M, Steil MC, Drache M, Conflant P (2000) J Solid State Chem 155:273
15. Lazarraga MG, Pico F, Amarilla JM, Rojas RM, Rojo JM (2005) Solid State Ionics 176:2313
16. Watanabe A (2002) J Solid State Chem 169:60
17. Watanabe A, Sekita M (2005) Solid State Ionics 176:2429
18. Abrahams I, Krok F, Chan SCM, Wrobel W, Kozanecka-Szmigiel A, Luma A, Dygas JR (2006) J Solid State Electr 10:569
19. Abrahams I, Kozanecka-Szmigiel A, Krok F, Wrobel W, Chan SCM, Dygas JR (2006) Solid State Ionics 177:1761
20. Shannon RD (1976) Acta Cryst A32:751
21. Watanabe A, Ishizawa N, Kato M (1985) J Solid State Chem 60:252
22. Hsieh CY, Fung KZ (2008) J Phys Chem Solids 69:302